^{64}Cu PET Imaging of the CXCR4 Chemokine Receptor Using a Cross-Bridged Cyclam Bis-Tetraazamacrocyclic Antagonist

Benjamin P. Burke*[1–3], Cecilia S. Miranda*[2,3], Rhiannon E. Lee[1,2], Isaline Renard[1,2], Shubhanchi Nigam[2,3], Gonçalo S. Clemente[2,3], Thomas D'Huys[4], Torsten Ruest[3], Juozas Domarkas[1,2], James A. Thompson[2,5], Timothy J. Hubin[6], Dominique Schols[4], Christopher J. Cawthorne*[2,3], and Stephen J. Archibald[1–3]

[1]Department of Chemistry, University of Hull, Hull, United Kingdom; [2]Positron Emission Tomography Research Centre, University of Hull, Hull, United Kingdom; [3]Department of Biomedical Sciences, University of Hull, Hull, United Kingdom; [4]Rega Institute for Medical Research, KU Leuven, Leuven, Belgium; [5]Hull York Medical School, University of Hull, Hull, United Kingdom; and [6]Department of Chemistry and Physics, Southwestern Oklahoma State University, Weatherford, Oklahoma

Expression of the chemokine receptor chemokine C-X-C motif receptor 4 (CXCR4) plays an important role in cancer metastasis, in autoimmune diseases, and during stem cell–based repair processes after stroke and myocardial infarction. Previously reported PET imaging agents targeting CXCR4 suffer from either high nonspecific uptake or bind only to the human form of the receptor. The objective of this study was to develop a high-stability ^{64}Cu-labeled small-molecule PET agent for imaging both human and murine CXCR4 chemokine receptors. **Methods:** Synthesis, radiochemistry, stability and radioligand binding assays were performed for the novel tracer ^{64}Cu-CuCB-bicyclam. In vivo dynamic PET studies were performed on mice bearing U87 (CXCR4 low-expressing) and U87.CXCR4 (human-CXCR4 high-expressing) tumors. Biodistribution and receptor blocking studies were performed on CD1-IGS immunocompetent mice. CXCR4 expression on tumor and liver disaggregates was confirmed using a combination of immunohistochemistry, quantitative polymerase chain reaction, and Western blot. **Results:** ^{64}Cu-CuCB-bicyclam has a high affinity for both the human and the murine variants of the CXCR4 receptor (half-maximal inhibitory concentration, 8 nM [human]/2 nM [murine]) and can be obtained from the parent chelator that has low affinity. In vitro and in vivo studies demonstrate specific uptake in CXCR4-expressing cells that can be blocked by more than 90% using a higher-affinity antagonist, with limited uptake in non–CXCR4-expressing organs and high in vivo stability. The tracer was also able to selectively displace the CXCR4 antagonists AMD3100 and AMD3465 from the liver. **Conclusion:** The tetraazamacrocyclic small molecule ^{64}Cu-CuCB-bicyclam has been shown to be an imaging agent for the CXCR4 receptor that is likely to be applicable across a range of species. It has high affinity and stability and is suitable for preclinical research in immunocompetent murine models.

Key Words: CXCR4; ^{64}Cu; azamacrocycle; cyclam; AMD3100

J Nucl Med 2020; 61:123–128
DOI: 10.2967/jnumed.118.218008

Chemokine C-X-C motif receptor 4 (CXCR4) is a 7-transmembrane helix G-protein–coupled receptor. The interaction of CXCR4 with its cognate ligand, stromal cell–derived factor 1α (SDF-1α/CXCL12), is essential during embryonic development and plays a key role in normal physiologic function, including control of hematopoietic cells during homeostasis (*1*). CXCR4 is overexpressed in multiple cancer types, with expression levels associated with increased proliferation, migration, and survival (*2,3*). In addition, CXCR4 expression on circulating tumor cells has been shown to enable metastasis to CXCL12-expressing organs, including liver, lung, and bone marrow (*4*), and inhibition of CXCR4/CXCL12 signaling reduces metastasis in various breast cancer models (*5*). There is a clear role in multiple myeloma, particularly in extramedullary disease, a chemotherapy-resistant subtype with poor prognosis (*6,7*). Important links have been elucidated between CXCL12 and immunotherapies, where blocking the signaling axis prevented recruitment of immunosuppressing fibroblast activation protein–positive stromal cells (*8*). CXCR4 has also been shown to have a role in stroke, autoimmune disease (*9,10*), and myocardial infarction, with CXCL12 upregulated after infarction (*11–13*). CXCR4 is therefore a candidate prognostic biomarker for several clinical indications. Because several CXCR4-targeted agents are currently in clinical trials, CXCR4 also has potential as a predictive biomarker to enable patient stratification.

The ^{68}Ga-radiolabeled cyclic peptide CPCR4.2 (*14,15*), pentixafor, has been used to demonstrate the potential of CXCR4 PET imaging over the past few years. Pentixafor has been used clinically to image human CXCR4 expression in a range of cancer types, including lymphoma, multiple melanoma, glioblastoma, and small cell lung cancer in proof-of-concept studies (*16–21*). However, pentixafor has little or no binding affinity to the murine variant of CXCR4 (*18*), limiting assessment of nonxenogenic CXCR4 expression in preclinical models.

Small-molecule CXCR4 antagonists based on tetraazamacrocycles, including AMD3100 and AMD3465 (*22*) (Supplemental Fig. 1; supplemental materials are available at http://jnm.snmjournals.org), bind to both the human and the mouse variants of the receptor (*23–26*), with AMD3100 the sole CXCR4 antagonist currently approved by the U.S. Food and Drug Administration and the European Medicines Agency for human use. The cyclam components of these molecules allow for transition metal complex formation, which switches the binding mode from electrostatic/H-bonding between

Received Sep. 20, 2018; revision accepted Jun. 3, 2019.
For correspondence or reprints contact: Stephen J. Archibald, University of Hull, Cottingham Rd., Hull, HU6 7RX, United Kingdom.
E-mail: s.j.archibald@hull.ac.uk
*Contributed equally to this work.
Published online Jun. 14, 2019.

the protonated cyclam amine groups and aspartate residue side chains (171 and 262) to coordinate bonds with the same residues. Direct labeling with ^{64}Cu to enable PET imaging has been attempted (*27–30*), and although CXCR4-dependent tumor uptake of ^{64}Cu-CuAMD3100 and ^{64}Cu-CuAMD3465 (Supplemental Fig. 1) has been demonstrated, high nonspecific hepatic accumulation (likely caused by complex instability) prevented further development of these compounds (*28,29*). Copper(II) cyclam complexes are unlikely to have sufficient kinetic stability to retain the metal ion in vivo (*31–38*).

Configurational restriction of the cyclam with an ethylene cross-bridge confers kinetic stability on the copper(II) complex and increases affinity for, and residence time at, the CXCR4 receptor. The ethylene bridge in the macrocyclic rings of CB-bicyclam (Fig. 1B) allows only 1 configuration for the macrocycle copper(II) complex, which optimizes coordinate bond formation with CXCR4 residues relative to nonbridged cyclam metal complexes of AMD3100 (*37,39–44*). The unbridged macrocycle complexes are in equilibrium between up to 6 possible configurations, leading to a stochastic overall affinity reflective of the average of these states. The affinity increase is likely mediated by reduction in bond lengths (effectively switched from axial to equatorial) to give shorter, stronger coordination bonds to CXCR4 receptor surface aspartate residues (*39,40*).

We have developed an understanding of structure–activity relationships of CXCR4-binding bridged azamacrocyclic compounds and set out to apply this knowledge to the development of PET imaging probes. Currently, there are no blockable and stable nuclear imaging agents that bind to both human and nonhuman variants of CXCR4, inhibiting research in syngeneic models or understanding of the role of CXCR4 in developmental pathways (*45*). In this work, we investigated a ^{64}Cu-labeled tetraazamacrocyclic small-molecule CXCR4 antagonist that has suitable characteristics (biodistribution, specificity, and stability) for imaging both the human and the murine homologs of the CXCR4 receptor.

MATERIALS AND METHODS

Ethics

All animal procedures were approved by the University of Hull Animal Welfare Ethical Review Body and performed in accordance with the United Kingdom's Guidance on the Operation of Animals (Scientific Procedures) Act of 1986 and within guidelines set out by the United Kingdom National Cancer Research Institute Committee on the Welfare of Animals in Cancer Research under Home Office Project License number 60/4549 held by Dr. Cawthorne (*46*).

General

All chemicals were supplied by Sigma-Aldrich unless otherwise stated and were used as supplied. Elemental analysis was performed using a carbon, hydrogen, and nitrogen analyzer (EA1108; Carlo Erba). Accurate mass spectrometry measurements were obtained using a linear-trap-quadropole device (Orbitrap XL; Thermo Fisher Scientific). Semipreparative high-performance liquid chromatography was performed using an Agilent 1100 series device equipped with an ultraviolet light detector (series G1314A) and a NaI radiodetector. Thin-layer chromatography was performed using neutral alumina sheets (Merck), eluting with 95:5 methanol:water, saturated with excess NaCl. Radio–thin-layer chromatography was performed using a Lablogic ScanRam, equipped with a NaI detector at a speed of 10 mm/min. Data were recorded using Lablogic Laura (version 4.1.13.91). ^{64}Cu was purchased from the University of Cambridge. Further details of synthesis, radiochemistry, and stability methodologies are presented in Supplemental Figures 2 and 3. ^{64}Cu-CuAMD3100 was synthesized and analyzed following a reported procedure (*27*).

Cell Lines

The U87 cell line was purchased from American Type Culture Collection, and the glioblastoma astrocytoma U87.CD4 cell line was transfected with human CXCR4 or murine CXCR4. Both U87 and U87.CXCR4 (human and murine) cells were grown in Dulbecco modified Eagle medium, with L-glutamine medium (Lonza) with U87.CXCR4 supplemented by a 2 μg/mL concentration of puromycin. All cell lines were cultured in the presence of 10% fetal bovine serum, in a humidified incubator with 5% CO_2. The intracellular calcium mobilization in response to CXCL12 was measured in human U87.CXCR4 cell lines at 37°C by monitoring the fluorescence of an intracellular calcium probe (Fig. 1A) as a function of time using a fluorometric imaging plate reader (Molecular Devices) (*40,47*), with compounds (AMD3100, CuAMD3100, CB-bicyclam, CuCB-bicyclam, and Cu_2CB-bicyclam) tested in the concentration range 0.01–10,000 nM. Flow cytometry was performed as previously described using a FACSCalibur (Becton Dickinson), and data were analyzed using CellQuest software (Becton Dickinson) (*39*). CXCR4 expression was determined by Western blot, immunohistochemistry (as previously described) (*15,28*), and quantitative polymerase chain reaction (as previously described; Supplemental Table 1).

Receptor Binding Assay

Human U87.CXCR4 cells grown to 60%–80% confluence were used for receptor binding

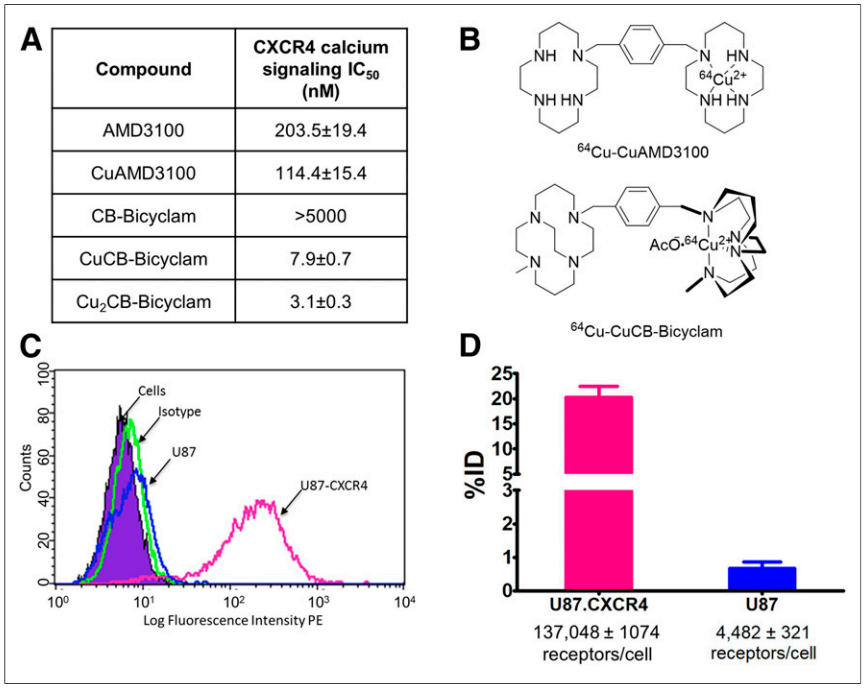

FIGURE 1. In vitro assessment of ^{64}Cu-CuCB-bicyclam. (A) Comparative affinity values vs. CXCL12 determined by calcium flux assay. (B) Chemical structures of ^{64}Cu-CuAMD3100 and ^{64}Cu-CuCB-bicyclam. (C) Fluorescence-activated cell sorting determination of CXCR4 expression. (D) Binding of ^{64}Cu-CuCB-bicyclam on U87 and U87.CXCR4-expressing cell lines.

assays. Cells were washed with cold phosphate-buffered saline (PBS), and flasks were placed on ice to prevent receptor internalization. Cells were detached using a cell scraper and centrifuged at 200*g* for 5 min; 5×10^5 cells were then resuspended with cold PBS. Cells were incubated with ^{64}Cu-CuCB-bicyclam (37 kBq/mL; 5.2 nM) in PBS for 60 min at 4°C. After incubation, cells were washed quickly 3 times with cold PBS and cell-associated radioactivity was determined in using an automatic γ-counter (Wizard 3″; Wallac).

For blocking experiments, cells were preincubated with 20 μM Cu_2CB-bicyclam for 1 h before being washed 3 times in cold PBS buffer and incubated with radiotracer as above. Data are expressed as percentage incubated dose ± SEM, representing the mean of 3 independent experiments with 3 internal repeats.

Animal Models

Female CD1-IGS (Crl:CD1(ICR)) and CD1-Nude (Crl:CD1-*Foxn1*^{Nu}) mice (aged 21–27 d; weight, 20–25 g) were purchased from Charles River Laboratories. CD1-Nude mice were subcutaneously implanted with a 5×10^6 cell/100 μL suspension of U87/U87-human CXCR4 cells in Geltrex (Life Technologies) basement membrane in the upper flank, under anesthesia. Tumor sizes were measured every 2 d using calipers, and tumor volume (mm^3) was determined as length × width × height.

PET/CT Imaging and Analysis

Dynamic whole-body PET and CT images were acquired on a SuperArgus 2R PET scanner (Sedecal). Anesthesia was induced with 5% isoflurane/oxygen (v/v) and then maintained at 2%, using a flow rate of 1 L/min. After cannulation of the tail vein using a bespoke catheter, the mice were placed into an imaging cell where temperature and respiration were monitored (Minerve). ^{64}Cu-CuCB-bicyclam (8.9 ± 3.2 MBq, 7.15 GBq/μmol, 1.2 nmol) was injected at the beginning of a 90-min dynamic imaging sequence (10 frames: 3 × 120 s, 1 × 240 s, 4 × 600 s, and 2 × 1,200 s). The mice were kept at 1% anesthesia during scanning, with temperature and respiration monitored throughout. After the PET scan, a CT image was acquired for anatomic coregistration (40 kV, 140 μA, 360 projections, 8 shots).

For specificity studies, a separate group of mice was injected with a 5 mg/kg blocking dose of Cu_2CB-bicyclam administered intraperitoneally 60 min before injection of ^{64}Cu-CuCB-bicyclam.

PET emission data were reconstructed using 3-dimensional ordered-subset expectation maximization with corrections for randoms, scatter. and attenuation. Data were analyzed using AMIDE (*48*) and Vivoquant software (InVicro), with regions of interest drawn over tumors and various tissues to generate time–activity curves. SUVs were obtained after correction for injected dose and animal weight. Tumor and liver samples were taken at sacrifice and fixed in formalin or frozen in liquid nitrogen.

Ex Vivo Biodistribution, Urine Stability, and Blocking Studies

CD1-IGS mice were injected intraperitoneally with a 5 mg/kg dose of Cu_2CB-bicyclam, CuCB-bicyclam, AMD3100, or AMD3465 in saline. For control experiments, no blocking injection was given. At 60 min after blocking, the mice were injected intravenously with approximately 740 kBq of ^{64}Cu-CuCB-bicyclam (or ^{64}Cu-AMD3100) in the tail vein, and this stock solution was used to calibrate the automatic γ-counter (Wizard 3″). At 90 min after tracer injection, blood, brain, heart, plasma, muscle, lungs, thymus, bone, spleen, nose, kidney, liver, and intestines were collected after sacrifice and dissection. Radioactivity within tissue samples was counted using the automatic γ-counter, and counts per minute for each tissue sample were normalized to the total injected dose of radioactivity and weight of tissue to give the radioactivity uptake as percentage injected dose (%ID)/g. Before sacrifice, urine was collected and analyzed by radio–thin-layer chromatography using the same quality control method as during synthesis to determine stability (*27*).

Data Analysis

Uptake was compared between U87 (CXCR4 low-expressing) and U87.CXCR4 (human CXCR4 high-expressing) tumors via an unpaired 2-tailed *t* test. Tumor and liver uptake was compared in blocked and nonblocked animals via an unpaired 1-tailed *t* test. *P* values of less than 0.05 were considered to be statistically significant.

RESULTS

Synthesis and Characterization

The nonradioactive analog CuCB-bicyclam was formed by reacting the previously described CB-bicyclam with a stoichiometric amount of copper(II) acetate to form the mono-copper derivative, after which analytically pure samples were obtained using size-exclusion chromatography (Supplemental Fig. 2) (*39*). The in vitro binding affinity of the mono-copper complex to both human and murine CXCR4 was determined via a CXCL12-stimulated calcium flux signaling assay, and the half-maximal inhibitory concentration was determined to be 8 nM (human CXCR4), whereas the free chelator precursor CB-bicyclam displayed no measurable activity in this assay (>5 μM) (Supplemental Fig. 4). Similar results were observed for murine CXCR4, with a half-maximal inhibitory concentration of 2 nM for CuCB-bicyclam in a murine CXCL12 binding assay (Supplemental Fig. 5).

Radiochemistry, Purification, and Stability

^{64}Cu-CuCB-bicyclam was radiochemically synthesized by heating CB-bicyclam with preformed ^{64}Cu-$Cu(OAc)_2$ and monitoring via radio–thin-layer chromatography (Supplemental Fig. 3). On full incorporation (40–50 min), the crude complex was purified of excess CB-bicyclam using semipreparative high-performance liquid chromatography to give decay-corrected isolated radiochemical yields of 69% ± 5% with a total synthesis time of 120 min and a specific activity of 7.15 GBq/μmol. The LogP value was −2.38 ± 0.18. ^{64}Cu-CuAMD3100 was synthesized and analyzed following previously published procedures (*28*). In vitro acid stability was measured to indicate comparative stability between tracers by incubation in 6 M $HClO_4$ for 3 h at 37°C. Radio–thin-layer chromatography methods identical to those used to analyze the radiosynthesis process were applied, and stability values of 92% ± 3% and 9% ± 5% were determined for ^{64}Cu-CuCB-bicyclam and ^{64}Cu-CuAMD3100, respectively.

Receptor Expression and ^{64}Cu-CuCB-Bicyclam Radioligand Binding In Vitro

CXCR4 surface expression levels were determined by fluorescence-activated cell sorting for U87 and U87.CXCR4 cells (ca. 4,000 vs. 148,000 receptors per cell, respectively) (Fig. 1). Radioligand binding experiments showed ratios similar to the expression level for binding of the tracer (0.66% ± 0.56% and 20.22% ± 5.78% applied dose for U87 and U87.CXCR4 cells, respectively) (Fig. 1). Preincubation of U87.CXCR4 cells with Cu_2CB-bicyclam (half-maximal inhibitory concentration, 3 nM) decreased binding of ^{64}Cu-CuCB-bicyclam by 89%, consistent with high specific uptake.

PET/CT Studies on Tumor-Bearing Mice

Dynamic PET/CT studies performed on U87 and U87.CXCR4 xenograft–bearing mice demonstrated significantly higher uptake in U87.CXCR4 tumors than in U87 tumors after administration of ^{64}Cu-CuCB-bicyclam (9.6 ± 0.7 MBq), with an SUV_{max} of 7.36% ± 1.77% versus 0.80% ± 0.14% at 80–90 min after injection (Fig. 2). Tumor-to-muscle ratios at 90 min after injection were 23.6 ± 2.7 for U87.CXCR4 tumors and 3.0 ± 0.5 for U87 tumors. Uptake was

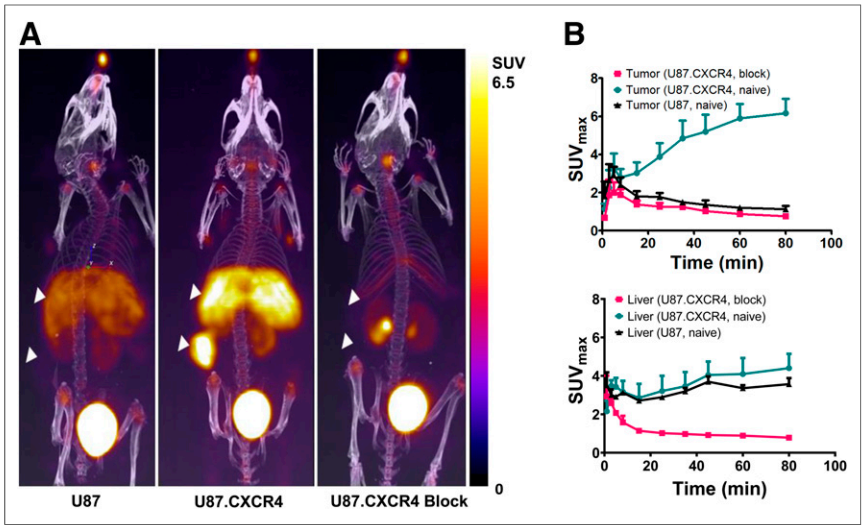

FIGURE 2. In vivo PET/CT evaluation of ^{64}Cu-CuCB-bicyclam. (A) Fused PET/CT maximum-intensity projections at 70–90 min after injection from CD1 mice bearing U87-CXCR4 (n = 3), U87 (n = 3), and U87.CXCR4 block (n = 2). Animals were injected with 9.6 ± 0.7 MBq of ^{64}Cu-CuCB-bicyclam. A 5 mg/kg blocking dose of Cu_2CB-bicyclam was given 1 h before ^{64}Cu-CuCB-bicyclam injection where indicated. Arrows denote position of tumor and liver. (B) Dynamic tumor time–activity curve for showing uptake of ^{64}Cu-CuCB-bicyclam in tumor (top) and liver (bottom) during 90 min. Data represent mean uptake of 2–3 animals ± SEM. *U87.CXCR4 vs. U87, $P < 0.01$. **Block vs. naïve, $P < 0.01$. Supplemental Figures 6 and 7 show all images at 70–90 min and time–activity curves for bladder, kidney, and vena cava.

also seen in the kidneys and liver. Injection of a 5 mg/kg dose of Cu_2CB-bicyclam 60 min before scanning reduced U87.CXCR4 tumor and liver uptake by more than 90%. Supplemental Figures 6 and 7 present all scan data and further analysis.

Ex Vivo Analysis of CXCR4 Expression

CXCR4 expression in U87.CXCR4 and U87 tumors and murine liver was confirmed ex vivo by a combination of Western blot, immunohistochemistry, and quantitative polymerase chain reaction (Supplemental Fig. 8; Supplemental Table 1).

Biodistribution and Tracer Stability Studies in Immunocompetent Mice

Biodistribution studies were performed using CD1-IGS mice at 90 min to determine the effect of a functional immune system on tracer distribution (Fig. 3). Low uptake (<2 %ID/g) was noted in all organs except kidney (8.11 %ID/g) and organs known to express CXCR4 (spleen [4.71 %ID/g], lung [2.89 %ID/g], and liver [13.77 %ID/g]). Urine was analyzed from a separate cohort of animals injected with ^{64}Cu-CuCB-bicyclam and ^{64}Cu-CuAMD3100 before sacrifice. ^{64}Cu-CuCB-bicyclam was more than 90% intact, whereas less than 10% of ^{64}Cu-CuAMD3100 remained intact in the urine.

Using murine liver CXCR4-dependent uptake of ^{64}Cu-CuCB-bicyclam as a readout, the in vivo affinities or residence times of Cu_2CB-bicyclam, CuCB-bicyclam, AMD3100, and AMD3465 were compared. Doses were administered 60 min before tracer administration, and animals were sacrificed at several time points after injection to provide tissue for biodistribution. Consistent with PET imaging in CD1-Nude mice, predosing with the Cu_2CB-bicyclam significantly reduced tracer uptake at 60 min in liver (3.40 vs. 13.77 %ID/g, $P < 0.05$), spleen (0.48 vs. 4.71 %ID/g, $P < 0.01$), and lungs (1.06 vs. 2.89 %ID/g, $P < 0.05$) but not 12 h; similar results were seen using CuCB-bicyclam. No significant decrease in liver uptake was seen when animals were preinjected with AMD3100 or AMD3465 at any time point.

DISCUSSION

This study reports a high-affinity CXCR4-specific PET imaging agent (^{64}Cu-CuCB-bicyclam) that binds selectively and with high stability to both the human and the murine variants of the CXCR4 receptor. Although ^{64}Cu-CuCB-bicyclam has potential as a clinical diagnostic PET imaging agent for oncology, it also represents a useful tool for the interrogation of CXCR4 expression levels over time in genetically engineered or immunocompetent preclinical models, useful in the investigation of CXCR4-targeting synergy with immunomodulatory therapies (*49*).

Unlike AMD3100 and AMD3465, the labeling precursor CB-bicyclam has CXCR4 affinity of more than 5 μM because alkylation of the secondary amines disrupts the hydrogen-bonding potential. The monocopper species CuCB-bicyclam has a higher affinity to the CXCR4 receptor than either AMD3100 or CuAMD3100 but lower than our previously described bis-copper species (Cu_2CB-bicyclam). However, the affinity is likely to be sufficient for imaging studies, and ^{64}Cu-CuCB-bicyclam has the advantage of a precursor with more than 100-fold lower receptor affinity. ^{64}Cu radiolabeling was performed using the minimum concentration required for full radiometal incorporation. We chose to purify ^{64}Cu-CuCB-bicyclam from unreacted CB-bicyclam using semipreparative high-performance liquid chromatography for these experiments.

Radioligand binding experiments using U87.CXCR4 and U87 cells showed specific binding, with binding correlating well with quantified surface expression levels of CXCR4. In addition, in vitro binding could be blocked using the higher-affinity complex Cu_2CB-bicyclam. In vivo PET/CT imaging using U87.CXCR4 and U87 tumor–bearing mice mirrored the in vitro binding results, with selective high uptake in U87.CXCR4 tumors at 90 min after injection. In vivo specificity was confirmed using a blocking dose of the higher-affinity Cu_2CB-bicyclam, which reduced U87.CXCR4 tumor uptake by more than 90%.

As seen in previous studies using ^{64}Cu-labeled macrocycles for CXCR4 imaging, moderate liver uptake was seen on PET imaging using ^{64}Cu-CuCB-bicyclam. This uptake was reduced after blocking with Cu_2CB-bicyclam (5 mg/kg) to an extent comparable to that of U87.CXCR4 tumors, suggesting specific binding to CXCR4. This finding is comparable to previous studies in which very high doses of AMD3100 (50 mg/kg) were used for blocking (*33*). Murine liver expression of CXCR4 was confirmed after ex vivo disaggregation of tumor or liver at the protein level via fluorescence-activated cell sorting and immunohistochemistry. Further experiments demonstrated that more than 90% of urine radioactivity was intact ^{64}Cu-CuCB-bicyclam, whereas most activity from ^{64}Cu-CuAMD3100–injected animals was in the form of free ^{64}Cu ions. Acid stability assays (6 M $HClO_4$) showed similar

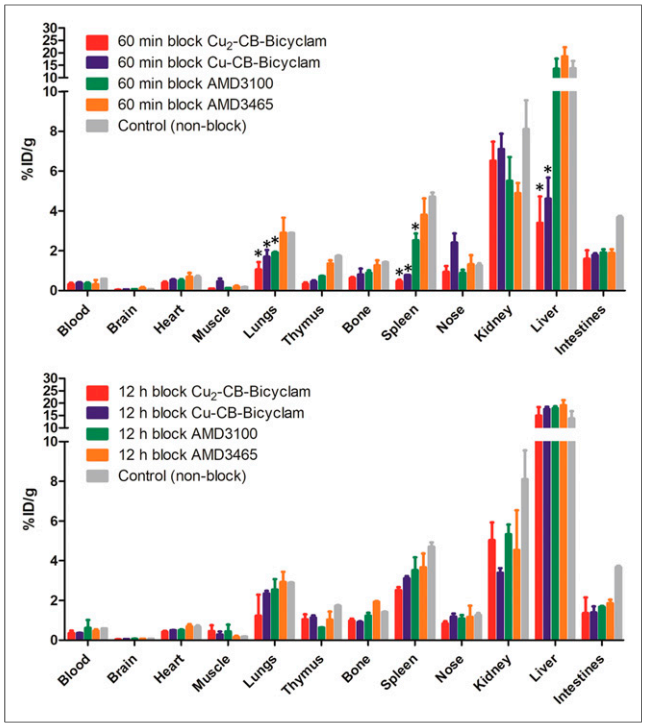

FIGURE 3. Assessment of in vivo uptake of ^{64}Cu-CuCB-bicyclam after blocking with range of CXCR4 antagonists. Biodistribution of selected tissues from CD1-IGS mice given 5 mg/kg dose of Cu_2CB-bicyclam, CuCB-bicyclam, AMD3100, or AMD3465 60 min (top) or 12 h (bottom) before ^{64}Cu-CuCB-bicyclam injection. Tissue was harvested 90 min after tracer administration ($n = 4$). *Block vs. naïve, $P < 0.05$.

profiles for stability. These data are consistent with in vitro studies, demonstrating that cyclam copper(II) complexes that do not possess either structural reinforcement or coordinating arms have rapid binding kinetics but low stability in competition experiments (*31,50,51*). These data confirm not only the insufficient stability of any nonbridged or nonfunctionalized cyclam-based copper(II) complex for in vivo PET imaging applications but also the higher stability of cross-bridged cyclam structures.

Further biodistribution studies were performed using immunocompetent mice to study the effect of blocking with various CXCR4 antagonists on the uptake of ^{64}Cu-CuCB-bicyclam. As expected, liver uptake of the tracer could be blocked by administration of either the higher-affinity Cu_2CB-bicyclam or CuCB-bicyclam at 60 min before tracer administration. However, tracer uptake could not be blocked by the lower-affinity CXCR4 antagonists AMD3100 and AMD3465 (Fig. 3; Supplemental Table 2). This observation could be explained by shorter (i.e., <60 min) receptor residence times for the unbridged cyclam compounds or displacement of AMD3100 or AMD3465 from CXCR4 by the higher-affinity ^{64}Cu-CuCB-bicyclam compound (*30*). Although the development of therapeutic agents targeting CXCR4 was not the focus of this study, the high stability, high affinity, and appropriate biodistribution of ^{64}Cu-CuCB-bicyclam create interest in exploring the identical radioactive and nonradioactive analogs as an imaging–chemotherapeutic pair. The ^{67}Cu derivative is of interest for investigating a radionuclide theranostic approach (*52*), assuming that the CXCR4-related liver uptake is lower in humans than in mice.

CONCLUSION

In this study we have developed a ^{64}Cu-labeled configurationally restricted azamacrocyclic CXCR4 antagonist with high affinity and stability and with favorable biodistribution characteristics. To our knowledge, ^{64}Cu-CuCB-bicyclam is the first CXCR4-targeted PET imaging agent that has suitable characteristics for routine imaging studies and binds to both the human and the murine CXCR4 receptor variants. This agent allows wider preclinical assessment of the role of CXCR4 in syngeneic tumor models and immunocompetent models and will be useful for translation to other animal models of disease that require imaging of the endogenous CXCR4 receptor.

DISCLOSURE

Funding was provided by the Daisy Appeal Charity (grant DAhul0211 and BPB fellowship) and by Yorkshire Cancer Research (HEND376). The University of Hull provided studentship funding to Rhiannon Lee and Cecilia Miranda. No other potential conflict of interest relevant to this article was reported.

ACKNOWLEDGMENTS

We gratefully acknowledge Dr. Assem Allam and his family for the generous donation to help found the PET Research Centre at the University of Hull. Mass spectrometry data were acquired at the EPSRC U.K. National Mass Spectrometry Facility at Swansea University.

KEY POINTS

QUESTION: The goal of this study was to develop a configurationally restricted azamacrocyclic compound as a high-affinity and high-stability ^{64}Cu radiotracer for imaging CXCR4 chemokine receptor expression in mice and humans.

PERTINENT FINDINGS: The radiotracer ^{64}Cu-CuCB-bicyclam binds with high affinity to both murine and human CXCR4. The compound retains the ^{64}Cu radiolabel and is excreted intact, with blocking studies in vivo showing significantly reduced uptake in liver, in spleen, and in human CXCR4–expressing tumor.

IMPLICATIONS FOR PATIENT CARE: ^{64}Cu-CuCB-bicyclam is an appropriate tracer for studies of murine CXCR4 expression in mouse models and can be translated for use in humans.

REFERENCES

1. Zou YR, Kottmann AH, Kuroda M, Taniuchi I, Littman DR. Function of the chemokine receptor CXCR4 in haematopoiesis and in cerebellar development. *Nature.* 1998;393:595–599.
2. Balkwill F. The significance of cancer cell expression of the chemokine receptor CXCR4. *Semin Cancer Biol.* 2004;14:171–179.
3. Yoon Y, Liang ZX, Zhang Y, et al. CXC chemokine receptor-4 antagonist blocks both growth of primary tumor and metastasis of head and neck cancer in xenograft mouse models. *Cancer Res.* 2007;67:7518–7524.
4. Burger JA, Kipps TJ. CXCR4: a key receptor in the crosstalk between tumor cells and their microenvironment. *Blood.* 2006;107:1761–1767.
5. Singh B, Cook KR, Martin C, et al. Evaluation of a CXCR4 antagonist in a xenograft mouse model of inflammatory breast cancer. *Clin Exp Metastasis.* 2010;27:233–240.
6. Nervi B, Ramirez P, Rettig MP, et al. Chemosensitization of acute myeloid leukemia (AML) following mobilization by the CXCR4 antagonist AMD3100. *Blood.* 2009;113:6206–6214.
7. Roccaro AM, Mishima Y, Sacco A, et al. CXCR4 regulates extra-medullary myeloma through epithelial-mesenchymal-transition-like transcriptional activation. *Cell Reports.* 2015;12:622–635.

8. Feig C, Jones JO, Kraman M, et al. Targeting CXCL12 from FAP-expressing carcinoma associated fibroblasts synergizes with anti-PD-L1 immunotherapy in pancreatic cancer. *Proc Natl Acad Sci USA.* 2013;110:20212–20217.
9. Hummel S, Van Aken H, Zarbock A. Inhibitors of CXC chemokine receptor type 4: putative therapeutic approaches in inflammatory diseases. *Curr Opin Hematol.* 2014;21:29–36.
10. Ruscher K, Kuric E, Liu YW, et al. Inhibition of CXCL12 signaling attenuates the postischemic immune response and improves functional recovery after stroke. *J Cereb Blood Flow Metab.* 2013;33:1225–1234.
11. Ghadge SK, Muhlstedt S, Ozcelik C, Bader M. SDF-1 alpha as a therapeutic stem cell homing factor in myocardial infarction. *Pharmacol Ther.* 2011;129:97–108.
12. Kitaori T, Ito H, Schwarz EA, et al. Stromal cell-derived factor 1/CXCR4 signaling is critical for the recruitment of mesenchymal stem cells to the fracture site during skeletal repair in a mouse model. *Arthritis Rheum.* 2009;60:813–823.
13. Kucia M, Dawn B, Hunt G, et al. Cells expressing early cardiac markers reside in the bone marrow and are mobilized into the peripheral blood after myocardial infarction. *Circ Res.* 2004;95:1191–1199.
14. Demmer O, Gourni E, Schumacher U, Kessler H, Wester H-J. PET imaging of CXCR4 receptors in cancer by a new optimized ligand. *ChemMedChem.* 2011;6: 1789–1791.
15. Gourni E, Demmer O, Schottelius M, et al. PET of CXCR4 expression by a ^{68}Ga-labeled highly specific targeted contrast agent. *J Nucl Med.* 2011;52:1803–1810.
16. Herrmann K, Lapa C, Wester HJ, et al. Biodistribution and radiation dosimetry for the chemokine receptor CXCR4-targeting probe ^{68}Ga-pentixafor. *J Nucl Med.* 2015;56:410–416.
17. Philipp-Abbrederis K, Herrmann K, Knop S, et al. In vivo molecular imaging of chemokine receptor CXCR4 expression in patients with advanced multiple myeloma. *EMBO Mol Med.* 2015;7:477–487.
18. Wester HJ, Keller U, Schottelius M, et al. Disclosing the CXCR4 expression in lymphoproliferative diseases by targeted molecular imaging. *Theranostics.* 2015;5:618–630.
19. Lapa C, Luckerath K, Kleinlein I, et al. Ga-68-pentixafor-PET/CT for imaging of chemokine receptor 4 expression in glioblastoma. *Theranostics.* 2016;6:428–434.
20. Lapa C, Luckerath K, Rudelius M, et al. Ga-68 pentixafor-PET/CT for imaging of chemokine receptor 4 expression in small cell lung cancer: initial experience. *Oncotarget.* 2016;7:9288–9295.
21. Vag T, Gerngross C, Herhaus P, et al. First experience with chemokine receptor CXCR4-targeted PET imaging of patients with solid cancers. *J Nucl Med.* 2016;57: 741–746.
22. Woodard LE, De Silva RA, Azad BB, et al. Bridged cyclams as imaging agents for chemokine receptor 4 (CXCR4). *Nucl Med Biol.* 2014;41:552–561.
23. Wong RSY, Bodart V, Metz M, Labrecque J, Bridger G, Fricker SP. Comparison of the potential multiple binding modes of bicyclam, monocylam, and noncyclam small-molecule CXC chemokine receptor 4 inhibitors. *Mol Pharmacol.* 2008;74: 1485–1495.
24. Bodart V, Anastassov V, Darkes MC, et al. Pharmacology of AMD3465: a small molecule antagonist of the chemokine receptor CXCR4. *Biochem Pharmacol.* 2009;78:993–1000.
25. De Clercq E. Recent advances on the use of the CXCR4 antagonist plerixafor (AMD3100, Mozobil (TM)) and potential of other CXCR4 antagonists as stem cell mobilizers. *Pharmacol Ther.* 2010;128:509–518.
26. Debnath B, Xu SL, Grande F, Garofalo A, Neamati N. Small molecule inhibitors of CXCR4. *Theranostics.* 2013;3:47–75.
27. Jacobson O, Weiss ID, Szajek L, Farber JM, Kiesewetter DO. ^{64}Cu-AMD3100: a novel imaging agent for targeting chemokine receptor CXCR4. *Bioorg Med Chem.* 2009;17:1486–1493.
28. Nimmagadda S, Pullambhatla M, Stone K, Green G, Bhujwalla ZM, Pomper MG. Molecular imaging of CXCR4 receptor expression in human cancer xenografts with [^{64}Cu]AMD3100 positron emission tomography. *Cancer Res.* 2010;70:3935–3944.
29. De Silva RA, Peyre K, Pullambhatla M, Fox JJ, Pomper MG, Nimmagadda S. Imaging CXCR4 expression in human cancer xenografts: evaluation of monocyclam ^{64}Cu-AMD3465. *J Nucl Med.* 2011;52:986–993.
30. Weiss ID, Jacobson O, Kiesewetter DO, et al. Positron emission tomography imaging of tumors expressing the human chemokine receptor CXCR4 in mice with the use of ^{64}Cu-AMD3100. *Mol Imaging Biol.* 2012;14:106–114.
31. Boswell CA, Sun XK, Niu WJ, et al. Comparative in vivo stability of copper-64-labeled cross-bridged and conventional tetraazamacrocyclic complexes. *J Med Chem.* 2004;47:1465–1474.
32. Hubin TJ, McCormick JM, Collinson SR, Alcock NW, Busch DH. Ultra rigid cross-bridged tetraazamacrocycles as ligands: the challenge and the solution. *Chem Commun.* 1998;(16):1675–1676.
33. Lewis EA, Boyle RW, Archibald SJ. Ultrastable complexes for in vivo use: a bifunctional chelator incorporating a cross-bridged macrocycle. *Chem Commun (Camb).* 2004;(19):2212–2213.
34. Mewis RE, Archibald SJ. Biomedical applications of macrocyclic ligand complexes. *Coord Chem Rev.* 2010;254:1686–1712.
35. Silversides JD, Allan CC, Archibald SJ. Copper(II) cyclam-based complexes for radiopharmaceutical applications: synthesis and structural analysis. *Dalton Trans.* 2007;971–978.
36. Silversides JD, Smith R, Archibald SJ. Challenges in chelating positron emitting copper isotopes: tailored synthesis of unsymmetric chelators to form ultra stable complexes. *Dalton Trans.* 2011;40:6289–6297.
37. Sun X, Wuest M, Weisman GR, et al. Radiolabeling and in vivo behavior of copper-64-labeled cross-bridged cyclam ligands. *J Med Chem.* 2002;45:469–477.
38. Woodin KS, Heroux KJ, Boswell CA, et al. Kinetic inertness and electrochemical behavior of copper(II) tetraazamacrocyclic complexes: possible implications for in vivo stability. *Eur J Inorg Chem.* 2005;4829–4833.
39. Khan A, Nicholson G, Greenman J, et al. Binding optimization through coordination chemistry: CXCR4 chemokine receptor antagonists from ultrarigid metal complexes. *J Am Chem Soc.* 2009;131:3416–3417.
40. Maples RD, Cain AN, Burke BP, et al. Aspartate-based CXCR4 chemokine receptor binding of cross-bridged tetraazamacrocyclic copper(II) and zinc(II) complexes. *Chemistry.* 2016;22:12916–12930.
41. McRobbie G, Valks GC, Empson CJ, et al. Probing key coordination interactions: configurationally restricted metal activated CXCR4 antagonists. *Dalton Trans.* 2007;5008–5018.
42. Smith R, Huskens D, Daelemans D, et al. CXCR4 chemokine receptor antagonists: nickel(II) complexes of configurationally restricted macrocycles. *Dalton Trans.* 2012;41:11369–11377.
43. Valks GC, McRobbie G, Lewis EA, et al. Configurationally restricted bismacrocyclic CXCR4 receptor antagonists. *J Med Chem.* 2006;49:6162–6165.
44. Liang X, Weishaupl M, Parkinson JA, Parsons S, McGregor PA, Sadler PJ. Selective recognition of configurational substrates of zinc cyclam by carboxylates: implications for the design and mechanism of action of anti-HIV agents. *Chemistry.* 2003;9:4709–4717.
45. Weiss ID, Jacobson O. Molecular imaging of chemokine receptor CXCR4. *Theranostics.* 2013;3:76–84.
46. Workman P, Aboagye EO, Balkwill F, et al. Guidelines for the welfare and use of animals in cancer research. *Br J Cancer.* 2010;102:1555–1577.
47. Princen K, Hatse S, Vermeire K, De Clercq E, Schols D. Evaluation of SDF-1/CXCR4-induced Ca2+ signaling by fluorometric imaging plate reader (FLIPR) and flow cytometry. *Cytometry A.* 2003;51:35–45.
48. Loening AM, Gambhir SS. AMIDE: a free software tool for multimodality medical image analysis. *Mol Imaging.* 2003;2:131–137.
49. D'Alterio C, Nasti G, Polimeno M, et al. CXCR4-CXCL12-CXCR7, TLR2-TLR4, and PD-1/PD-L1 in colorectal cancer liver metastases from neoadjuvant-treated patients. *Oncoimmunology.* 2016;5:e1254313.
50. Wadas TJ, Wong EH, Weisman GR, Anderson CJ. Copper chelation chemistry and its role in copper radiopharmaceuticals. *Curr Pharm Des.* 2007;13:3–16.
51. Wei L, Ye Y, Wadas TJ, et al. Cu-64-labeled CB-TE2A and diamsar-conjugated RGD peptide analogs for targeting angiogenesis: comparison of their biological activity. *Nucl Med Biol.* 2009;36:277–285.
52. Blower PJ. A nuclear chocolate box: the periodic table of nuclear medicine. *Dalton Trans.* 2015;44:4819–4844.